Effects R^{3+} on the photoluminescent properties of $Ca_2R_8(SiO_4)_6O_2$:A (R = Y,La,Gd;A = Eu^{3+},Tb^{3+}) phosphor films prepared by the sol–gel process

2004 J. Phys.: Condens. Matter 16 2745

(http://iopscience.iop.org/0953-8984/16/15/024)

INSTITUTE OF PHYSICS PUBLISHING JOURNAL OF PHYSICS: CONDENSED MATTER

J. Phys.: Condens. Matter **16** (2004) 2745–2755 PII: S0953-8984(04)72849-0

Effects R^{3+} on the photoluminescent properties of $Ca_2R_8(SiO_4)_6O_2$:A (R = Y, La, Gd; A = Eu^{3+}, Tb^{3+}) phosphor films prepared by the sol–gel process

X M Han, J Lin[1], H L Zhou, M Yu, Y H Zhou and M L Pang

Key Laboratory of Rare Earth Chemistry and Physics, Changchun Institute of Applied Chemistry, Chinese Academy of Sciences, Changchun 130022, People's Republic of China

E-mail: jlin@ns.ciac.jl.cn

Received 1 December 2003, in final form 2 March 2004
Published 2 April 2004
Online at stacks.iop.org/JPhysCM/16/2745
DOI: 10.1088/0953-8984/16/15/024

Abstract

Using $CaCO_3$, metal oxides (all dissolved by nitric acid) and tetraethoxysilane $Si(OC_2H_5)_4$ (TEOS) as the main starting materials, $Ca_2R_8(SiO_4)_6O_2$:A (R = Y, La, Gd; A = Eu^{3+}, Tb^{3+}) phosphor films have been dip-coated on quartz glass substrates through the sol–gel process. X-ray diffraction (XRD), atomic force microscope (AFM), scanning electron microscope (SEM) and photoluminescence (PL) spectra as well as lifetimes were used to characterize the resulting films. The results of XRD indicated that the 1000 °C annealed films are isomorphous and crystallize with the silicate oxyapatite structure. AFM and SEM studies revealed that the phosphor films consisted of homogeneous particles ranging from 30 to 90 nm, with an average thickness of 1.30 μm. The Eu^{3+} and Tb^{3+} show similar spectral properties independent of R^{3+} in the films due to their isomorphous crystal structures. However, both the emission intensity and lifetimes of Eu^{3+} and Tb^{3+} in $Ca_2R_8(SiO_4)_6O_2$ (R = Y, La, Gd) films decrease in the sequence of R = Gd > R = Y > R = La, which have been explained in accordance with the crystal structures.

(Some figures in this article are in colour only in the electronic version)

1. Introduction

There is growing interest in thin film phosphors due to their potential application in high-resolution devices such as cathode ray tubes and flat panel display devices [1]. The displays with thin film phosphors have higher contrast and resolution, superior thermal conductivity, higher degree of uniformity and better adhesion (to the substrates) than those made from

[1] Author to whom any correspondence should be addressed.

powder phosphors [2–5]. Thin phosphor films have been prepared by a variety of deposition techniques, such as chemical vapour deposition [6], spray pyrolysis [7] and pulsed laser deposition [8]. Generally, these techniques need expensive and complicated equipment setups. Therefore, a simple and economical method for making high quality thin film phosphors is desirable. The solution-based sol–gel method is one of the most important techniques for the synthesis of various functional coating films because it possesses a number of advantages over conventional film formation techniques, such as low temperature processing, easy coating of large surfaces, and possible formation of porous films and homogeneous multicomponent oxide films [9]. In fact, some efforts have been made to develop various kinds of luminescent films via sol–gel method in the past decade. Representative examples are Y_2SiO_5:Tb [2] and $Y_3Al_5O_{12}$:Tb [1] films for cathodoluminescence, $Y_3Al_5O_{12}$:Eu [10] films for field emission displays, Y_2O_3:Eu [11] and Zn_2SiO_4:Mn [12] films for photoluminescence.

Compounds with the apatite structure are very suitable host lattices for various luminescent ions. The most well known example is Sb^{3+} and Mn^{2+}-coactivated calcium halophosphate $Ca_5(PO_4)_3(F, Cl)$:Sb, Mn, which has found applications in fluorescent lamps for a long time [13]. $Ca_2R_8(SiO_4)_6O_2$ (R = Y, Gd, La) is a kind of ternary rare-earth-metal silicate with the oxyapatite structure, which has been used as host materials for the luminescence of various rare earth and mercury-like ions [14–16]. The most prominent structural characteristics are the two sites in the oxyapatite host lattice, i.e. the nine-coordinated 4f site with C_3 point symmetry and the seven-coordinated 6h site with C_S point symmetry [15]. Both sites are very suitable for the luminescence of rare earth ions (f–f transitions) due to their low symmetry features. Recently, we reported on the luminescence properties of Eu^{3+}, Tb^{3+} and Ce^{3+} in the binary $La_{9.33}(SiO_4)_6O_2$ oxyapatite films [17]. As a series study on the silicate oxyapatite phosphor films, in this paper we report on the luminescent properties of two rare earth ions (Eu^{3+}, Tb^{3+}) in the ternary rare-earth-metal silicate oxyapatite $Ca_2R_8(SiO_4)_6O_2$ (R = Y, Gd, La) phosphor films prepared by sol–gel process, with an emphasis on the effects R^{3+} ions on the luminescence properties of the phosphor films.

2. Experimental section

Thin film phosphor samples of $Ca_2R_8(SiO_4)_6O_2$:A (R = Y, La, Gd; A = Eu^{3+}, Tb^{3+}) were prepared by a sol–gel and dip-coating process [18]. The starting materials were $CaCO_3$ (analytical reagent, AR), R_2O_3 (R = Y, La, Gd, 99.99%), Eu_2O_3 (99.99%), Tb_4O_7 (99.99%) and $Si(OC_2H_5)_4$ (TEOS). A stoichiometric amount of the above rare earth oxides and $CaCO_3$ were dissolved in diluted HNO_3 (AR), then mixed with a water–ethanol (v/v = 1:4) solution. A stoichiometric amount of $Si(OC_2H_5)_4$ (TEOS) was added with a total volume ratio of H_2O/TEOS = 1:1 in the solution. The thus obtained solution was stirred for 2 h to form a sol and dip-coated successively on thoroughly cleaned silica glass substrates at a speed of 0.2 cm s^{-1}. The as formed films were dried at 100 °C for 1 h immediately. Then the dried films were annealed to 1000 °C with a heating rate of 1 °C min^{-1} and held there for 2 h in air. For those films containing Tb^{3+}, the above annealing process was performed in a reducing atmosphere of 95% N_2 + 5% H_2 (volume ratio).

The x-ray diffraction (XRD) of the film samples was examined on a Rigaku-Dmax 2500 diffractometer using Cu Kα radiation (λ = 0.154 05 nm). The morphology of the crystalline films was inspected using an atomic force microscope (AFM, Nanoscope III A scanning probe microscopy from Digital Instruments) with a contact mode and scanning electron microscope (SEM, JEOL JXA-840). The excitation and emission spectra were taken on a Hitachi F-4500 spectrofluorimeter equipped with a 150 W xenon lamp as the excitation source. Luminescence lifetimes were measured with a SPEX 1934D phosphorimeter using a 7 W pulse xenon lamp

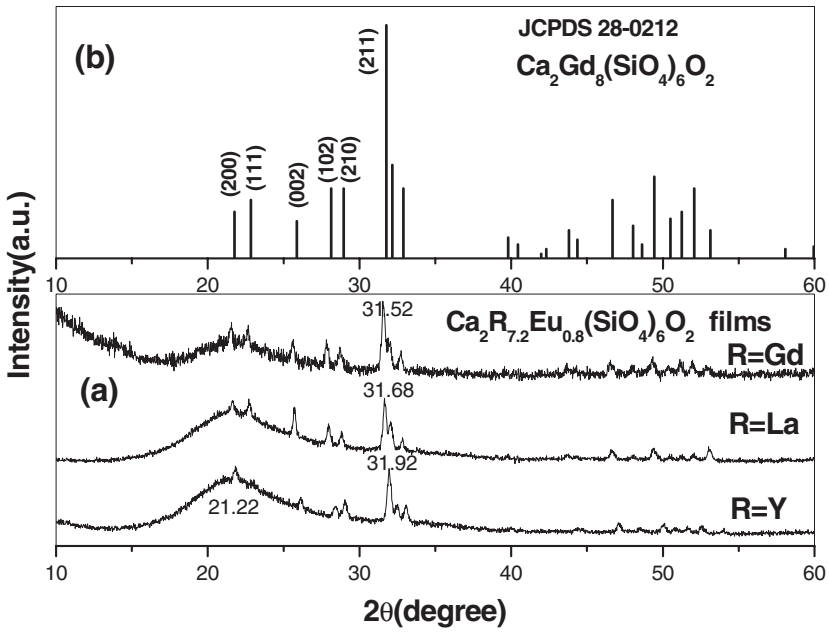

Figure 1. X-ray diffraction patterns for $Ca_2R_{7.2}Eu_{0.8}(SiO_4)_6O_2$ (R = Y, La, Gd) film samples annealed at 1000 °C (a) and the JCPDS Cards for $Ca_2Gd_8(SiO_4)_6O_2$ (no 28-0212) (b).

as the excitation source with the pulse width of 3 μs. All the measurements were performed at room temperature (RT).

3. Results

3.1. XRD and morphology of the phosphor films

Here we confine ourselves only to the $Ca_2R_{7.2}Eu_{0.8}(SiO_4)_6O_2$ (R = Y, La, Gd) series samples to elucidate the structure and morphology of the phosphor films. Figure 1 shows the XRD patterns for $Ca_2R_{7.2}Eu_{0.8}(SiO_4)_6O_2$ (R = Y, La, Gd) film samples annealed at 1000 °C and the JCPDS Cards (no 28-0212) for standard $Ca_2Gd_8(SiO_4)_6O_2$ as references. In figure 1(a) for all the three films, the broad band at $2\theta = 21.22°$ arises from the quartz glass substrates, and the other diffraction peaks are in good agreement with those of standard $Ca_2Gd_8(SiO_4)_6O_2$, indicating that all the films are isomorphous and crystallize with the oxyapatite structure. No second phase is detected.

The morphology of the crystalline $Ca_2R_{7.2}Eu_{0.8}(SiO_4)_6O_2$ (R = Y, La, Gd) films was inspected with an atomic force microscope (AFM) and a scanning electron microscope (SEM). Figure 2 shows the AFM images of the 1000 °C annealed $Ca_2Y_{7.2}Eu_{0.8}(SiO_4)_6O_2$ (a), $Ca_2La_{7.2}Eu_{0.8}(SiO_4)_6O_2$ (b) and $Ca_2Gd_{7.2}Eu_{0.8}(SiO_4)_6O_2$ (c) films. It is known from planar images that the films, which are uniform and crack-free, mainly consist of closely packed particles with an average grain size of 60 nm for $Ca_2Y_{7.2}Eu_{0.8}(SiO_4)_6O_2$ (figure 2(a)), 30 nm for $Ca_2La_{7.2}Eu_{0.8}(SiO_4)_6O_2$ (figure 2(b)) and 90 nm for $Ca_2Gd_{7.2}Eu_{0.8}(SiO_4)_6O_2$ (figure 2(c)), respectively. The film surface is well crystallized and very smooth with a root mean square (RMS) roughness of 9.77 nm for $Ca_2Y_{7.2}Eu_{0.8}(SiO_4)_6O_2$, 5.29 nm for $Ca_2La_{7.2}Eu_{0.8}(SiO_4)_6O_2$ and 9.13 nm for $Ca_2Gd_{7.2}Eu_{0.8}(SiO_4)_6O_2$. The SEM images of the surface and cross-section of $Ca_2Gd_{7.2}Eu_{0.8}(SiO_4)_6O_2$ film annealed at 1000 °C are shown in figures 3(a) and (b),

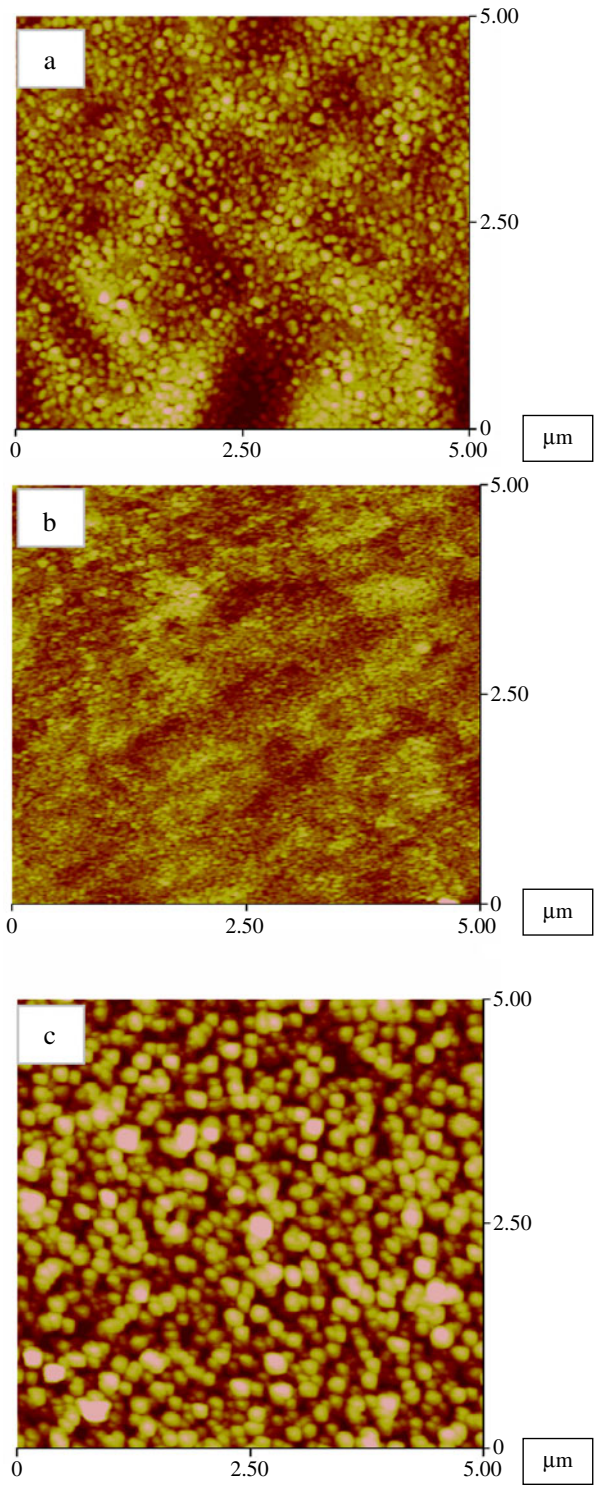

Figure 2. AFM micrographs for $Ca_2Y_{7.2}Eu_{0.8}(SiO_4)_6O_2$ (a), $Ca_2La_{7.2}Eu_{0.8}(SiO_4)_6O_2$ (b) and $Ca_2Gd_{7.2}Eu_{0.8}(SiO_4)_6O_2$ (c) phosphor films annealed at 1000 °C.

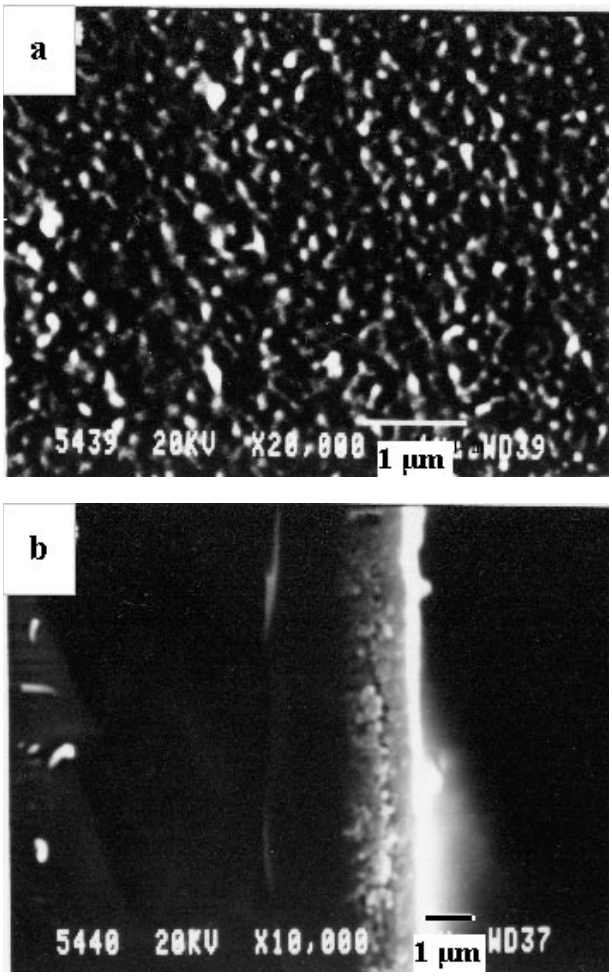

Figure 3. SEM micrographs of $Ca_2Gd_{7.2}Eu_{0.8}(SiO_4)_6O_2$ film annealed at 1000 °C. (a) Surface image, (b) cross-section image.

respectively. In agreement with the AFM image in figure 2(c), the surface SEM micrograph (figure 3(a)) also indicates that the particles in the $Ca_2Gd_{7.2}Eu_{0.8}(SiO_4)_6O_2$ film have an average size of 100 nm, and the cross-section SEM micrograph (figure 3(b)) shows that the film grown by successive dip-coating steps has an average thickness of 1.30 μm.

3.2. Dependence of the luminescence properties of A ($A = Eu^{3+}, Tb^{3+}$) on R^{3+} in $Ca_2R_8(SiO_4)_6O_2$ ($R = Y, La, Gd$) films

$Ca_2R_8(SiO_4)_6O_2:Eu^{3+}$ films. Figures 4(a) and (b) show the excitation and emission spectra for $Ca_2R_{7.2}Eu_{0.8}(SiO_4)_6O_2$ (R = Y, La, Gd) films annealed at 1000 °C, respectively. It is known from figure 4(a) that all three excitation spectra show strong absorption from 220 to 300 nm with maxima of 263 nm for R = Y, La and 276 nm for R = Gd due to the charge transfer transition of the Eu^{3+}–O^{2-} bond (CTB) [13, 18]. The sharp peak at 276 nm for R = Gd superimposed on Eu^{3+} CTB is due to a ^8S–^6I transition Gd^{3+} in the host lattice [18]. Excitation into the CTB at 263 nm yields the characteristic emission of Eu^{3+} $^5D_0$–^7F_J ($J = 0, 1, 2, 3, 4$),

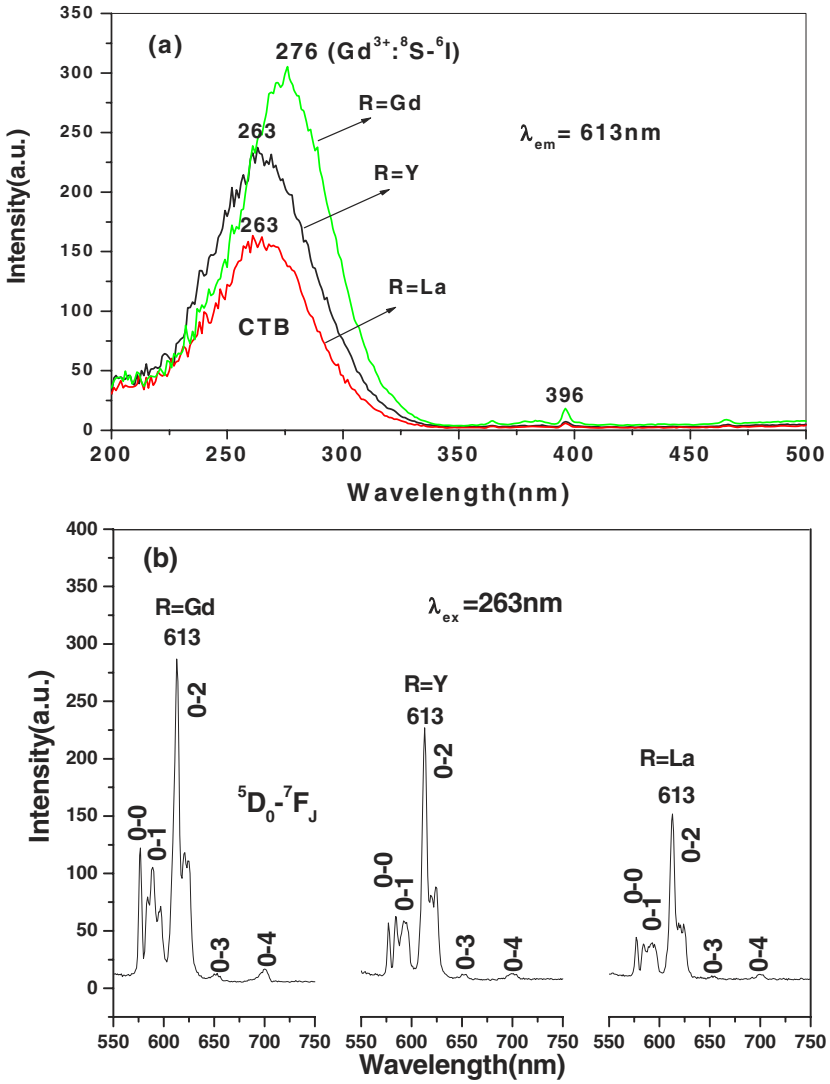

Figure 4. Excitation (a) and emission (b) spectra of $Ca_2R_{7.2}Eu_{0.8}(SiO_4)_6O_2$ (R = Y, La, Gd) films annealed at 1000 °C.

with the hypersensitive red emission transition $^5D_0$–$^7F_2$ (613 nm) being the most prominent group. The crystal splitting components of $^5D_0$–$^7F_1$ and $^5D_0$–$^7F_2$ of Eu^{3+} can be observed, but not totally resolved due to the weak experimental resolution. In addition, no emission from higher ^5D_J ($J > 0$) levels of Eu^{3+} is observed, and the integrated emission intensity of Eu^{3+} ($^5D_0$–^7F_J) decreases as I (R = Gd) > I (R = Y) > I (R = La).

The decay curves for Eu^{3+} in $Ca_2R_{7.2}Eu_{0.8}(SiO_4)_6O_2$ (R = Y, La, Gd) films are shown in figure 5. In general, all these curves can be well fitted into a single exponential function as $I = I_0 \exp[-t/\tau]$ (I_0 is the initial emission intensity for $t = 0$, τ is $1/e$ the lifetime), from which the lifetimes of Eu^{3+} are determined and shown inside figure 5. It can be seen that the lifetimes of Eu^{3+} decrease as τ (R = Gd, 1.74 ms) > τ (R = Y, 1.70 ms) > τ (R = La, 1.64 ms), the same sequence as the emission intensity.

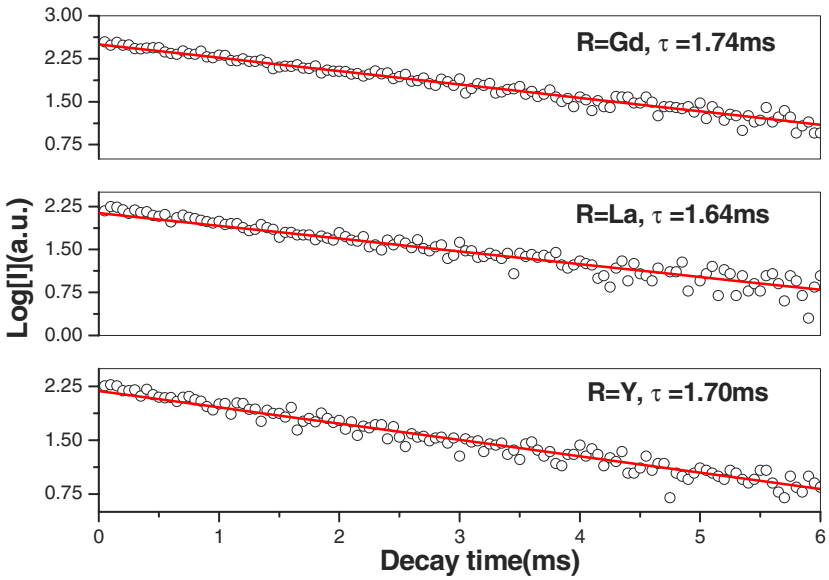

Figure 5. The decay curves for Eu^{3+} ($^5D_0$–$^7F_2$ at 613 nm) in $Ca_2R_{7.2}Eu_{0.8}(SiO_4)_6O_2$ (R = Y, La, Gd) films annealed at 1000 °C (points: experimental data; line: fitted results).

$Ca_2R_8(SiO_4)_6O_2$:Tb^{3+} films. The excitation and emission spectra of Tb^{3+} in $Ca_2R_{7.52}Tb_{0.48}(SiO_4)_6O_2$ (R = Y, La, Gd) films are shown in figures 6(a) and (b), respectively. Independent of R^{3+}, the excitation spectrum of Tb^{3+} (figure 6(a)) in $Ca_2R_{7.52}Tb_{0.48}(SiO_4)_6O_2$ films contains an intense broad band with a maximum at 233 nm due to the spin-allowed $4f^8$–$4f^75d$ transition [1, 13, 18]. The f–f excitation transitions of Tb^{3+} cannot be observed clearly due to their relatively weak intensity to the $4f^8$–$4f^75d$ transition. Additionally, for R = Gd the characteristic excitation lines of Gd^{3+} at 276 nm (^8S–^6I) and 316 nm (^8S–^6P) have been present in the excitation spectrum [18]. Excitation into the $4f^8$–$4f^75d$ band at 233 nm yields the characteristic blue emission $^5D_3$–^7F_J ($J = 3, 4, 5, 6$) and green emission $^5D_4$–^7F_J ($J = 3, 4, 5, 6$) lines of Tb^{3+} with the same order of magnitude in intensity (figure 6(b)). The profiles of the emission spectra of films are very similar and independent of R^{3+}, but integrated emission intensity of Tb^{3+} decreases as I (Gd) > I (Y) > I (La), the same sequence as that for the situation of Eu^{3+}. Additionally, a broad band (350–600 nm) superimposed on the narrow terbium emission lines has been observed in figure 6(b). This broad band also appeared in the emission spectra of the Eu^{3+} in the $Ca_2R_8(SiO_4)_6O_2$ films (not shown in figure 4(b)) and blank substrates, is due to the emission from the silica glass substrates.

Figure 7 shows the decay curves for the luminescence of Tb^{3+} ($^5D_4$–$^7F_5$ at 544 nm) in $Ca_2R_{7.52}Tb_{0.48}(SiO_4)_6O_2$ (R = Y, La, Gd) films. Independent of R^{3+} and similar to the situation of Eu^{3+}, all three curves can be fitted into a singly exponential function basically, and the lifetimes of Tb^{3+} are determined to be 3.00 ms for R = Gd, 2.22 ms for R = Y and 2.06 ms for R = La, which change in same the sequence as those for Eu^{3+}.

4. Discussion

The results of XRD indicate that all the films of $Ca_2R_8(SiO_4)_6O_2$:A (R = Y, La, Gd; A = Eu^{3+}) are isomorphous and crystallize with the silicate oxyapatite structure. In this kind of structure, two kinds of site are available for the cations, i.e. the nine-coordinated 4f site with C_3 point symmetry and the seven-coordinated 6h site with C_S point symmetry [16, 18].

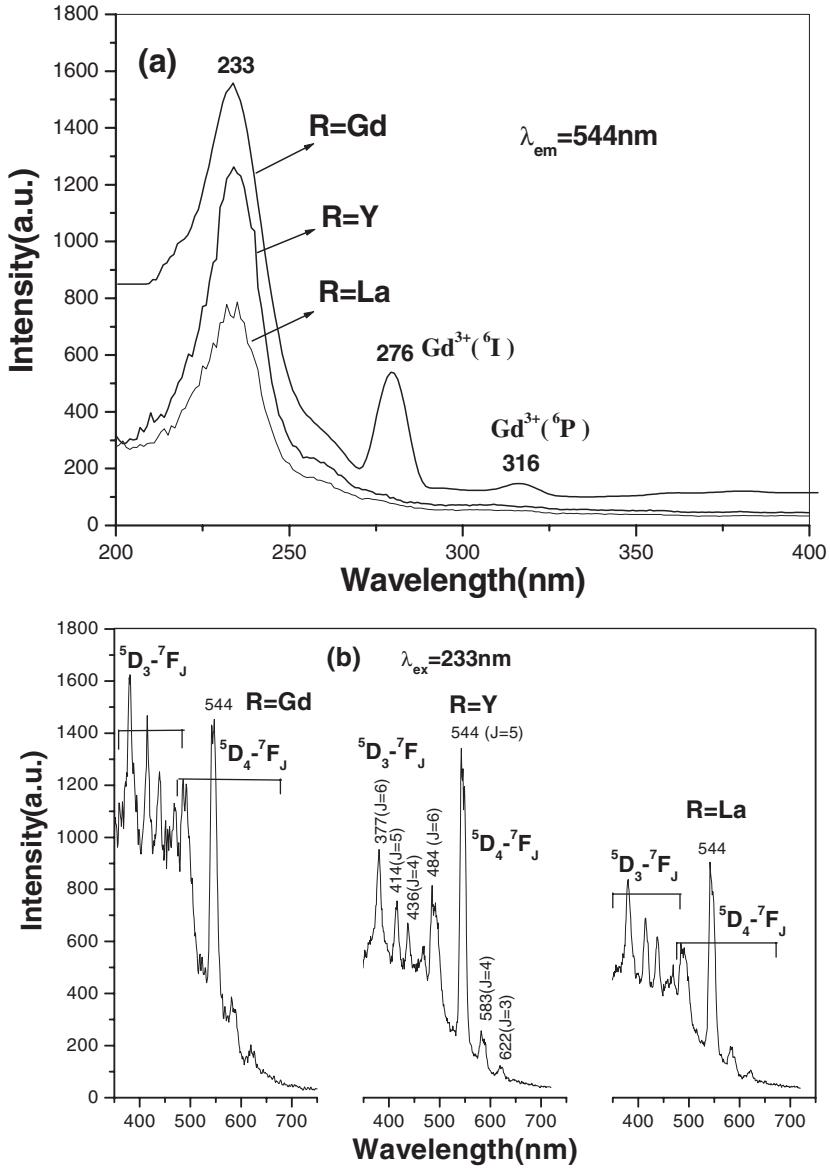

Figure 6. Excitation (a) and emission (b) spectra of $Ca_2R_{7.52}Tb_{0.48}(SiO_4)_6O_2$ (R = Y, La, Gd) film annealed at 1000 °C.

In $Ca_2R_8(SiO_4)_6O_2$, the two Ca^{2+} and two R^{3+} ions are located at four 4f sites, and the other six R^{3+} ions are distributed in six 6h sites [16]. Previous study by the high resolution emission spectra of Eu^{3+} indicated that the doped Eu^{3+} ions have occupied the 4f and 6h sites simultaneously in the ternary silicate oxyapatite powders [16]. Here we would not like to study this problem which needs laser excitation, and only confine ourselves to the effects of R^{3+} on the spectral and luminescence properties of Eu^{3+} and Tb^{3+} in $Ca_2R_8(SiO_4)_6O_2$ (R = Y, La, Gd) films.

First let us consider the spectral properties of Eu^{3+} in the films. In general, when the Eu^{3+} ion is located at the crystallographic site without inversion symmetry, its hypersensitive

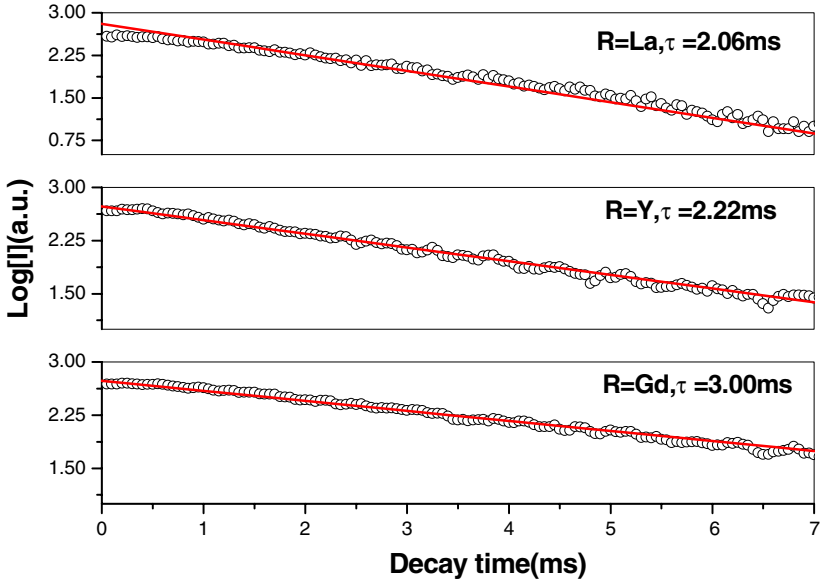

Figure 7. The decay curves for Tb^{3+} ($^5D_4$–$^7F_5$ at 544 nm) in $Ca_2R_{7.52}Tb_{0.48}(SiO_4)_6O_2$ (R = Y, La, Gd) films annealed at 1000 °C (points: experimental data; line: fitted results).

transition $^5D_0$–$^7F_2$ red emission will dominate in the emission spectrum; otherwise, if the Eu^{3+} site possesses an inversion centre, its $^5D_0$–$^7F_1$ (orange) emission will dominate [13, 17]. The spectral properties of Eu^{3+} are in good agreement with the crystal structure. In $Ca_2R_8(SiO_4)_6O_2$:Eu^{3+} (R = Y, La, Gd) films, the Eu^{3+} will replace the R^{3+} in view of their similar sizes and valence state. As a result, the Eu^{3+} is located at a site with C_3 and/or C_s point symmetry (without inversion centre). Thus its $^5D_0$–$^7F_2$ red (613 nm) emission presents as the most prominent group in all the three emission spectra (figure 4(b)). Also just due to this kind of symmetry for Eu^{3+}, its $^5D_0$–$^7F_0$ transition (around 577 nm) which only presents for Eu^{3+} in linear crystal field, appears with a relatively high intensity [19]. No emission from higher ^5D_J ($J > 0$) levels of Eu^{3+} is observed in the silicate oxyapatite films. This can be ascribed to the fact that the energy gaps between $^5D_2$ and $^5D_1$ and between $^5D_1$ and $^5D_0$ of Eu^{3+} are 2500 and 1750 cm^{-1}, respectively, and the silicate groups with maximum vibration energy of 950 cm^{-1} [20], are able to bridge the gaps between the higher lying levels of the Eu^{3+} and the $^5D_0$ level [13].

Secondly we will discuss the spectral properties of Tb^{3+} in the films. The Tb^{3+} can be used as an activator in green and blue phosphors. If the emission is mainly from the $^5D_3$ excited level, the emission colour is blue; if the emission is mainly from the $^5D_4$ excited level, the emission colour is green. The main factors influencing the relative intensity between $^5D_3$ and $^5D_4$ emission are the Tb^{3+} concentration and the vibration energy of the host lattice. At low concentrations it mainly emits blue light from the $^5D_3$ excited level, but at higher concentrations the $^5D_3$ emission will be quenched by cross relaxation ($^5D_3 + {}^7F_6 \rightarrow {}^5D_4 + {}^7F_0$), resulting in strong green emission from the $^5D_4$ excited level [13]. In $Ca_2R_{7.52}Tb_{0.48}(SiO_4)_6O_2$ (R = Y, La, Gd) films, both blue emission from the $^5D_3$ level and green emission from the $^5D_4$ level have been observed in the same order of magnitude. This is because the Tb^{3+} doping concentration is 6 at.% of R^{3+}, a relatively low value, and the cross relaxation cannot occur effectively. Furthermore, the maximum vibration energy of SiO_4 group is 950 cm^{-1} [20], which is five times less than the energy gap between $^5D_3$ and $^5D_4$ of Tb^{3+} (5600 cm^{-1}) [21], so the $^5D_3$

emission cannot be quenched by multiphonon relaxation efficiently. As a result, both emission from $^5D_3$ and $^5D_4$ levels has been observed in the same order of magnitude.

Now we shift to the emission intensity and lifetimes of Eu^{3+}, Tb^{3+} in the $Ca_2R_8(SiO_4)_6O_2$ (R = Y, La, Gd) film series. With the same doping concentration, it is found that both the emission intensity and lifetimes of Eu^{3+}, Tb^{3+} decrease in the sequence of R = Gd > R = Y > R = La. The Eu^{3+} and Tb^{3+} present the highest emission intensity and lifetimes in the films containing Gd^{3+}. This can be ascribed to the energy transfer from Gd^{3+} to Eu^{3+} and Tb^{3+}. In the excitation spectra of $Ca_2Gd_8(SiO_4)_6O_2$:Eu^{3+}/Tb^{3+} films (figures 4(a) and 6(a)), the excitation lines of Gd^{3+} (276 nm for ^8S–^6I and 316 nm for ^8S–^6P) can be seen clearly, indicating that an energy transfer occurs from Gd^{3+} to Eu^{3+} and Tb^{3+}. Upon excitation into the CTB (263 nm) of Eu^{3+} or $4f^8$–$4f^75d$ (233 nm) of Tb^{3+}, on the one hand the excitation energy can relax directly from these excited states to the 4f levels of Eu^{3+} and Tb^{3+} to yield their emission, on the other hand, excitation energy can also transfer to the 4f levels of Eu^{3+} and Tb^{3+} via the Gd^{3+}-sublattice to produce the emission. However, the latter energy transfer process cannot occur in $Ca_2Y_8(SiO_4)_6O_2$ and $Ca_2La_8(SiO_4)_6O_2$ films. As a result, the Eu^{3+} and Tb^{3+} are more efficiently excited and show higher emission intensity and longer lifetimes in $Ca_2Gd_8(SiO_4)_6O_2$ than in $Ca_2Y_8(SiO_4)_6O_2$ and $Ca_2La_8(SiO_4)_6O_2$ films.

Now we will elucidate why the Eu^{3+} and Tb^{3+} show higher emission intensity and longer lifetimes in $Ca_2Y_8(SiO_4)_6O_2$ than in $Ca_2La_8(SiO_4)_6O_2$ films. The ionic radii for Eu^{3+}, Tb^{3+}, Y^{3+}, La^{3+} are 0.947, 0.923, 0.90 and 0.103 nm (for six coordination), respectively [22], i.e. the ionic radii of Eu^{3+} and Tb^{3+} are larger than that of Y^{3+} but smaller than that of La^{3+}. After substitution for the Y^{3+} in $Ca_2Y_8(SiO_4)_6O_2$ film and the La^{3+} in $Ca_2La_8(SiO_4)_6O_2$ film, the Eu^{3+} and Tb^{3+} are expected to be in a stiff host lattice environment in the former but in a loose one in the latter. In other words, it can be said that more space is available for Eu^{3+}(Tb^{3+}) in $Ca_2La_8(SiO_4)_6O_2$ than in $Ca_2Y_8(SiO_4)_6O_2$ film host lattices. The stiffer the host lattice, the higher the emission intensity of the activator ions [23, 24]. It is expected that the expansion after excitation is not as strongly restricted by the surrounding of the luminescent ions in $Ca_2La_8(SiO_4)_6O_2$ film as in $Ca_2Y_8(SiO_4)_6O_2$ film. As a result, more nonradiative relaxations take place in $Ca_2La_8(SiO_4)_6O_2$ film than in $Ca_2Y_8(SiO_4)_6O_2$ film. Consequently, the Eu^{3+} and Tb^{3+} show higher emission intensity and longer lifetimes in $Ca_2Y_8(SiO_4)_6O_2$ than in $Ca_2La_8(SiO_4)_6O_2$ films. A very similar situation has been found for Eu^{3+} in other host lattices, such as YVO_4 and $LaVO_4$, i.e. under the same doping concentration the Eu^{3+} shows much higher emission intensity in YVO_4 than in $LaVO_4$ [25, 26].

5. Conclusions

Luminescent thin films of $Ca_2R_8(SiO_4)_6O_2$:A (R = Y, La, Gd; A = Eu^{3+}, Tb^{3+}) have been successfully deposited on quartz glass by the sol–gel dip coating method. The 1000 °C annealed films are uniform and crack free, which consist of grains with an average size of 30–90 nm depending on the film composition. The Eu^{3+} and Tb^{3+} show their characteristic emissions of $^5D_0$–^7F_J (J = 0, 1, 2, 3, 4) and $^5D_{3,4}$–^7F_J (J = 6, 5, 4, 3), respectively in the film hosts. With the same doping concentration, it is found that both the emission intensity and lifetimes of Eu^{3+}, Tb^{3+} decrease in the sequence of R = Gd > R = Y > R = La.

Acknowledgments

This project is financially supported by the foundation of 'Bairen Jihua' of Chinese Academy of Sciences, the MOST of China (no 2003CB314707), and the National Natural Science Foundation of China for Distinguished Young Scholars (50225205).

References

[1] Choe J Y, Ravichandran D, Biomquist S M, Morton D C, Kirchner K W, Ervin M H and Lee U 2001 *Appl. Phys. Lett.* **78** 3800
[2] Rabinovich E M, Shmulovich J, Fratello V J and Kopyov N J 1987 *Am. Ceram. Soc. Bull.* **6** 1505
[3] Robertson J M and van Tol M W 1980 *Appl. Phys. Lett.* **37** 471
[4] Fratello V J, Rabinovich E M and Shmulovich J 1990 *US Patent Specification* 4965091
[5] Lessard R B, Berglund K A and Nocera D G 1989 *Mater. Res. Soc. Symp. Proc.* **155** 119
[6] Bai G R, Zhang H and Foster C M 1998 *Thin Solid Films* **321** 115
[7] Hao J, Studenikin S A and Cocivera M 2001 *J. Lumin.* **93** 313
[8] Cho K G, Kumar D, Holloway P H and Singh R K 1998 *Appl. Phys. Lett.* **73** 3058
[9] Sakka S 1996 *Struct. Bond.* **85** 1
[10] Ravichandran D, Roy R, Chakhovskoi A G, Hunt C E, White W B and Erdei S 1997 *J. Lumin.* **71** 291
[11] Rao R P 1996 *Solid State Commun.* **99** 439
[12] Lin J, Saenger D U, Mennig M and Baerner K 2000 *Thin Solid Films* **360** 39
[13] Blasse G and Grabmaier B C 1994 *Luminescent Materials* (Berlin: Springer)
[14] Lin J and Su Q 1994 *Mater. Chem. Phys.* **38** 98
[15] Lin J and Su Q 1995 *J. Mater. Chem.* **5** 1151
[16] Lammers M J J and Blasse G 1987 *J. Electrochem. Soc.* **134** 2068
[17] Han X M, Lin J, Xing R B, Fu J, Wang S B and Han Y C 2003 *J. Phys.: Condens. Matter* **15** 2115
[18] Lin J and Su Q 1994 *J. Alloys Compounds* **210** 159
[19] Blasse G and Bril A 1966 *Philips Res. Rep.* **2** 368
[20] Yu M, Lin J, Zhou Y H, Wang S B and Zhang H J 2002 *J. Mater. Chem.* **12** 86
[21] Blasse G 1988 *Prog. Solid State Chem.* **18** 79
[22] Su Q 1992 *Rare Earth Chemistry* (Henan: Henan Science and Technology Press) (in Chinese)
[23] Verwey J W M and Blasse G 1990 *Mater. Chem. Phys.* **25** 91
[24] Lin J, Su Q, Zhang H and Wang S 1996 *Mater. Res. Bull.* **31** 189
[25] Ropp R C 1968 *J. Electrochem. Soc.* **115** 940
[26] Yu M, Lin J and Wang S B 2004 *Appl. Phys.* A at press